High Temperature Fast Response Aerodynamic Probe

Christian Lenherr
Department of Mechanical and Process
Engineering,
Laboratory for Energy Conversion,
ETH Zurich,
Sonneggstr.3,
8092 Zurich, Switzerland
e-mail: lenherr@lec.mavt.ethz.ch

Anestis I. Kalfas
Aristotle University of Thessaloniki,
School of Engineering,
54124 Thessaloniki, Greece

Reza S. Abhari
Department of Mechanical and Process
Engineering,
Laboratory for Energy Conversion,
ETH Zurich,
Switzerland

In order to advance the technology for measurements in higher temperature flows, a novel miniature (diameter 2.5 mm) fast response probe that can be applied in flows with temperatures of up to 533 K (500°F) has been developed. The primary elements of the probe are two piezoresistive pressure transducers that are used to measure the unsteady pressure and unsteady velocity field, as well as the steady temperature. Additional temperature and strain gauge sensors are embedded in the shaft to allow a much higher degree of robustness in the use of this probe. The additional temperature sensor in the shaft is used to monitor and correct the heat flux through the probe shaft, facilitating thermal management of the probe. The strain gauge sensor is used to monitor and control probe shaft vibration. Entirely new packaging technology had to be developed to make possible the use of this probe at such high temperatures. Extensive calibration and thermal cycling of the probe used to bind the accuracy and the robustness of the probe. This novel probe is applied in the one-and-1/2-stage, unshrouded axial turbine at ETH Zurich; this turbine configuration is representative of a high work aero-engine. The flow conditioning stretch upstream of the first stator is equipped with a recently designed hot streak generator. Several parameters of the hot streak, including temperature, radial and circumferential position, and shape and size can be independently controlled. The interactions between the hot streak and the secondary flow present a perfect scenario to verify the probe's capability to measure under real engine conditions. Therefore, measurements with the novel probe have been made in order to prove the principle and to detail the interaction effects with blade row pressure gradients and secondary flows.
[DOI: 10.1115/1.4001824]

1 Introduction

Measurement systems are not only used to investigate the operation of gas turbines, but are also of major importance in the development of control and diagnostics of modern turbomachinery. Therefore, the drive in recent years has been toward the accurate measurement of time dependent flow properties, such as pressure to gain more insight into phenomena, which vary over time and to feed back the gathered knowledge into new design processes [1–3]. But it is not only the design process that has been improved in recent decades. As predicted by several authors [4–8], significant progress has been made in areas such as the development of new materials and the improvement of cooling techniques, as well as in computational tools for the analysis and design of more powerful and efficient turbines. One of the main drivers for those improvements is related to the trend in higher inlet temperatures leading to a larger amount of work per unit mass flow and improvements in the weight-to-power ratio of gas turbines. Due to severe flow conditions at higher temperature levels, time-resolved measurements of flow properties such as pressure or temperature are still a major challenge.

Fast response aerodynamic probe (FRAP) technology has been developed at ETH Zurich and utilized extensively in the past for unsteady measurements of turbomachinery flow fields in a wide range of turbomachinery applications. Fast response pressure probes allow measurements of the flow angles, the Mach number, and the velocity and unlike complementary techniques, such as hotwire anemometry or laser techniques, it can also measure time-resolved static and total pressure. FRAP technology is based on piezoresistive miniature silicon sensors. The working principle of such sensors has been discussed in detail by several authors [3,9–14].

To date, however, FRAP technology has been limited to flow temperatures not exceeding 393 K [13,15,16]. The main limiting factors in terms of temperature are related to sensor limits, reduced signal to noise ratios, packaging issues, material issues, and electrical connections to the sensor.

This paper presents a newly developed miniature high temperature fast response aerodynamic probe (FRAP-HT), which can be applied in flows with temperatures up to 533 K (500°F), and demonstrates the use and the proof of the concept of the unsteady probe. The probe's robustness and ability to produce high frequency measurements in harsh environments are demonstrated with a hot streak generator equipped axial 1.5 stage turbine in the Axial Turbine Research Facility (LISA) facility.

2 High Temperature FRAP (F2S-HT)

First generation FRAP have been developed within the last 2 decades [2,15–18] in order to investigate unsteady flow phenomena such as secondary flows or rotor-stator interactions in turbomachinery [1,19–23]. Fast response aerodynamic probes satisfy all the given criteria for turbomachinery, such as a high measurement bandwidth of typically 5–12 kHz, a large Mach number range typically between 0.1 up to transonic, high spatial resolution, as well as a high measurement accuracy and easy access to the test section. The main challenges related to the development of a new high temperature FRAP probe are related to the sensor technology, signal conditioning, packaging technology, and electronic connections of the sensor within the probe.

Piezoresistive silicon pressure sensors are well-established and often used for fast response pressure applications. Their ability to measure the average component of pressure is one main advantage compared with piezoelectric sensors, which measure only the fluctuating component. The standard piezoresistive silicon sensors used for FRAP applications work as a Wheatstone bridge and are based on silicon strain gauge technology. The sensors used for the new probe are used in a differential mode with a linear pressure range of 900 mbar (Fig. 5). Their dimensions are length 2.2 mm

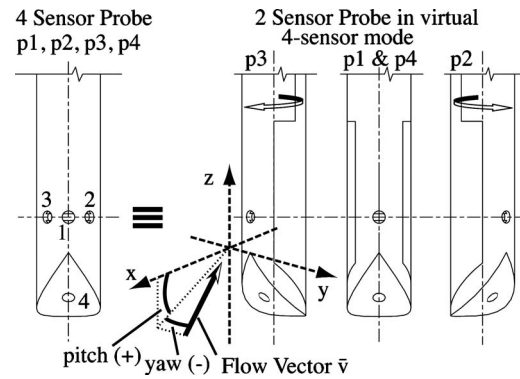**Fig. 1 FRAP-HT probe presented with a match for scale comparison**

Fig. 2 Yaw and pitch angle definition, including explanation of FRAP virtual four-sensor mode (stemwise rotation of the probe ±42 deg from the central position, p1)

by width 1.3 mm and a thickness of 0.4 mm. Due to their construction, full linearity is expected at least up to 473 K. Above that, the Wheatstone bridge still works, but some repeatable, non-linear behavior is expected due to leakage current flowing from p-type silicon elements into the n-type diaphragm material.

AlSi alloy bonding pads embedded on the sensor are the interface for the electronic connection to any power supply and signal conditioning device. The use of the classical gold wire bonding to the aluminum sensor pads is known to be critical for high temperature applications due to the formation of gold-aluminum intermetallic compounds and associated Kirkendall voids. The compounds are typically referred to as "purple plague." This term comes from the characteristic color of the $AuAl_2$ intermetallic compound that often occurs around the perimeter of Au bonded on an Al pad [24]. In general, such compounds occur if the time-temperature product is large enough (typically 448 K for 5–6 h) and grows at any time when high temperatures are encountered during the life of the device. The temporal change in the interface area due to further formation of the intermetallic compounds not only makes the connection more brittle but also influences the local resistance. In the worst case, this leads to a loss of connection. In order to avoid the formation of intermetallic compounds, the probe was designed so that aluminum ultrasonic wedge bonding is used to electrically connect the sensors.

In terms of packaging, the piezoresistive miniature silicon pressure sensors are directly embedded into the probe shaft. For a high temperature range of application it is very important to mechanically decouple the sensor from the base substrate to reduce mechanical stresses on the sensor membrane caused by the different thermal coefficients of expansions of the materials. Therefore, a dual component room-temperature-vulcanizing (RTV) silicon elastomer able to withstand temperatures up to 533 K is used as a soft bonding agent.

The cylindrical FRAP-HT probe head has a diameter of 2.5 mm. The pressure tap related to the yaw angle is 3.5 mm from the probe tip at an angle of 0 deg. The pitch sensitive tap is located 0.8 mm from the probe tip and at an angle of 45 deg from the probe axis on a shaped probe head (Fig. 1). The pitch sensitive as well as the yaw sensitive pressure tap hole diameter is 0.35 mm.

The primary elements of the probe are two piezoresistive pressure transducers that are used to measure the unsteady pressure and unsteady velocity field, as well as the steady temperature. Additional temperature and strain gauge sensors are embedded in the shaft to allow a much higher degree of robustness in the use of this probe. A protection shield is designed in the cavity of the probe pressure taps in order to further increase the probe robustness in harsh turbomachinery environments. This is even more important for industrial applications in order to prevent any damage to the probe tip and the sensors due to particle impacts. The two piezoresistive pressure transducers enable the measurement of the unsteady angles φ and γ, as well as P_{tot}, P_{stat}, and M, using the virtual four-sensor technique (Fig. 2). Furthermore, the flow temperature is measured on a steady way (10 Hz).

In the virtual four-sensor mode, the tap related to the yaw angle is used to measure the actual tap pressures in three consecutive steps (p1, p2, and p3) at the three different probe set-up angles (0

deg, −42 deg, +42 deg) relative to the probe stem central position, p1. The tap related to pitch angle is only used at the first step resulting in pressure, p4 (Fig. 2). These four consecutively measured independent pressure values are finally combined, referenced to a blade trigger, and used for the calculations of the different flow calibration coefficients for flow yaw and pitch angles, static, and total pressure, respectively.

2.1 Piezoresistive Sensor Calibration. The pressure sensor's working principle is the Wheatstone bridge (Fig. 5), which is fed by a constant current source of 1 mA. The excitation voltage Ue is mainly a measure of the membrane temperature and the signal voltage U is strongly proportional to the differential pressure across the membrane (Fig. 3). The raw signals are amplified in the probe box at the back end of the probe shaft by a factor of 100. The calibration procedure described in Kupferschmied [25] is applied to derive a sensor calibration model.

This work presents the first measurements conducted with the newly developed probe. The expected maximum temperature to phase during the measurements does not exceed 473 K. Therefore, the piezoresistive sensors behave dominantly linearly and the temperature window of 303 K to up to 473 K was used to define the sensor calibration coefficients. This results in a mean pressure sensitivity of 4.35 mV/(mbar mA) for both sensors and a mean temperature sensitivity of 0.38 mV/K for both sensors.

2.2 Steady Aerodynamic Probe Calibration. The steady aerodynamic calibration is based on traditional methods [15,26]. A set of four dimensionless calibration coefficients (Eq. (1)) is determined out of a freejet calibration, whereas p_{tot} and p_{stat} are values resulting out of operational information from the calibration tunnel. The spatial distribution of the calibration coefficients is presented in Fig. 4 for a calibration Mach number of 0.5.

$$K_\varphi = \frac{p_2 - p_3}{p_1 - p_m}; \quad K_\gamma = \frac{p_1 - p_4}{p_1 - p_m}; \quad K_t = \frac{p_{tot} - p_1}{p_1 - p_m}; \quad K_s = \frac{p_1 - p_{stat}}{p_1 - p_m}$$

(1)

where $p_m = (p_2 + p_3)/2$.

The resulting coefficient distribution is modeled by a two-dimensional polynomial. In the case of the FRAP-HT probe, this model is of the sixth order for both dimensions. The derived calibration model accuracy is given in Table 1 for a calibration range of ±24 deg in yaw and ±20 deg in pitch angles, respectively. The model accuracy is given in absolute values for the flow angles, as well as for total and static pressure. The accuracy for the Mach number is given as a percentage of the freejet calibration Mach number. Additionally, for total and static pressure, the accuracy is presented as a percentage of the real dynamic head at the freejet Mach number of 0.5.
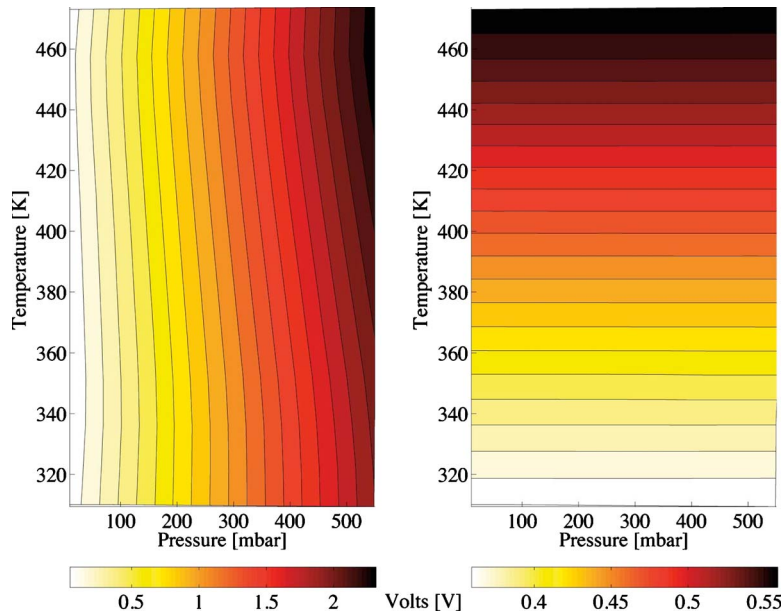
Fig. 3 Typical output signals, U (left) and Ue (right) in voltage (V), as a function of temperature and pressure, resulting from the probe sensor calibration

2.3 Dynamic Frequency Response. The dynamic behavior of FRAP probes is investigated through the transfer characteristics of each different component of interest. The sensor diaphragm and the sensor's position relative to the pressure tap are the main components influencing the dynamic response of the probe. The investigations of the sensor membrane response are carried out analytically, whereas the investigations related to the pressure tap and cavity size are experimental.

Fig. 4 Aerodynamic calibration coefficient curves for flow angles, K_φ and K_γ, and for total and static pressure, K_t and K_s; calibration range: yaw is ±24 deg and pitch is ±20 deg

Table 1 FRAP-HT calibration model accuracy for Ma=0.5 and calibration range ±24 deg for yaw and ±20 deg for pitch

Parameter	FRAP-HT accuracy	% of dynamic head
φ	±0.06 deg	
γ	±0.13 deg	
P_{tot}	±41 Pa	0.25
P_{stat}	±39 Pa	0.23
M	±0.18%	

2.3.1 Piezoresistive Miniature Silicon Chip. Due to design issues, the work of piezoresistive miniature silicon chips (Fig. 5) is almost lossless and typically shows very high natural frequencies (second order spring-mass system).

The natural frequency of the sensor membrane used is calculated by assuming an all-round clamped rectangular plate (Harris [27], p.7.36). This results in a natural frequency of the sensor membrane of 710 kHz. This very high value is explained by the small membrane thickness and width, as well as by the high aspect ratio between the modulus of elasticity and the mass density for silicon.

2.3.2 Pneumatic Cavity. The frequency response of a sensor usually deteriorates when assembled inside a probe and can vary slightly for every probe due to the complexity of the sensor assembly. The deterioration of the frequency response is related to the pneumatic cavity that occurs if the membrane is not flush-mounted. Numerous analytical approaches, for example, the organ pipe equation, have been applied in the past in order to calculate the frequency response of the pneumatic cavity [25]. These investigations showed that due to the complex cavity geometry, the simplified analytical models lead to deviations in the real eigenfrequencies of up to 30%.

Therefore, in order to validate the dynamic behavior of the probe, the sensor pressure signal of both sensors (yaw and pitch) has been measured in the freejet facility [25], equipped with a fine turbulent mesh grid. The resulting flow turbulence has constant amplitude over relatively low frequencies and then decays with a characteristic slope of $-5/3$ at higher frequencies. The normalized amplitude response $f^{5/3}PSD(f)$ versus frequency is shown in
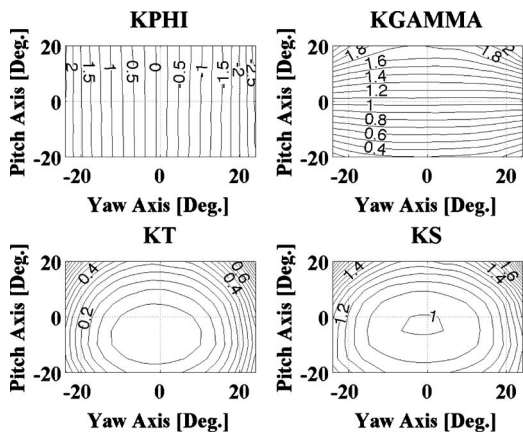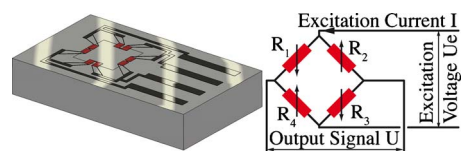

Fig. 5 Piezoresistive miniature silicon chip including electrical schematic of Wheatstone bridge working principle

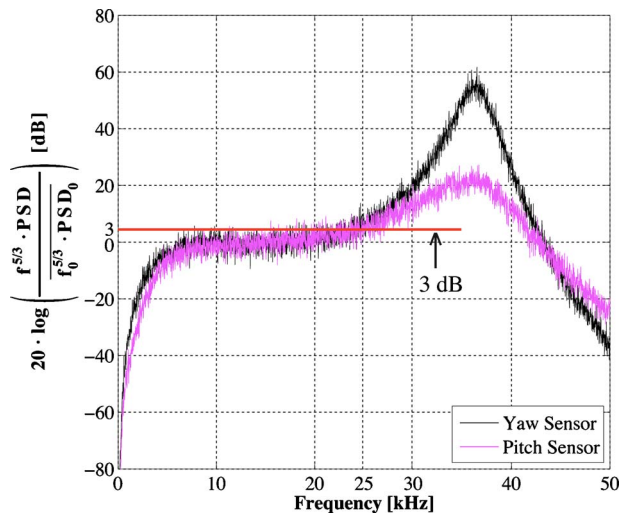**Fig. 6 Amplitude response of both sensors of the FRAP-HT probe: the measured response results from grid-generated turbulence**
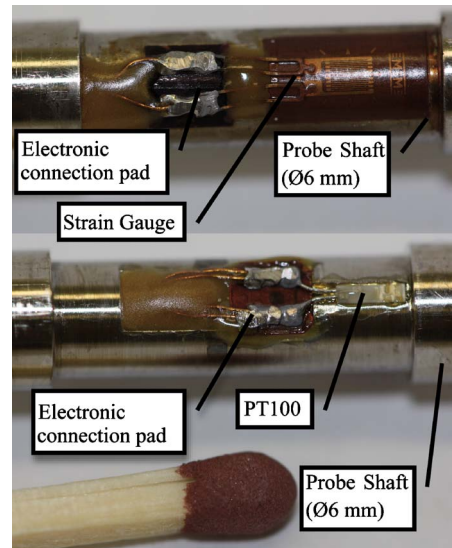

Fig. 7 Two views onto the same 6 mm FRAP-HT probe shaft presented with a match for scale comparison. The bottom view (PT100) shows the same shaft position as the top view (strain gauge) after a 180 deg stemwise rotation.

Fig. 6. The normalization is achieved by the mean of the amplitude response $f_0^{5/3}PSD_0$ over a frequency range of 8–18 kHz.

Both yaw and pitch sensors show similar dynamic behavior. The peaks at 36 kHz correspond to the eigenfrequency of the pneumatic cavity of the yaw and the pitch pressure tap, respectively. For both sensors the amplitude is flat up to a frequency of 25 kHz above which the amplitudes are in excess of 3 dB. Thus, the cut-off frequency of 25 kHz determines the measurement bandwidth of this probe.

2.4 Probe Shaft Temperature and Strain Gauge Sensor. An additional two sensors are installed on the 6 mm probe shaft, 100 mm behind the probe tip. The sensors are embedded in a slot around the circumference of the probe shaft. The slot depth is 0.5 mm and the circumference is separated into two areas in order to embed a strain gauge sensor on one of the semicylindrical planes and a PT100 temperature sensor on the other semicylindrical plane. The strain gauge sensor is used to monitor and control probe shaft vibration (Fig. 7, top). The temperature sensor in the shaft is used to monitor the heat flux through the probe shaft, allowing us to thermally manage the probe (Fig. 7, bottom).

3 Further Instrumentation

In order to prove the concept of the newly developed FRAP, comparisons of measurements between the new probe and the standard measurement equipment, such as traditional FRAP probes and pneumatic four-hole probes, are made. A short overview shall, therefore, be given about the measurement technologies applied in order to make the comparisons.

3.1 Standard Two-Sensor FRAP. The standard two-sensor FRAP technology has been used in recent years and a series of publications resulted from measurements conducted with that probe type (for instance, Refs. [28–31]). The probe has a similar head shape to the newly developed FRAP-HT but differs in its dimensions. The probe head has a diameter of 1.8 mm. The pressure tap related to the yaw angle is 2.8 mm from the probe tip at an angle of 0 deg. The pitch sensitive tap is located 0.6 mm from the probe tip and at an angle of 45 deg from the probe axis on a shaped probe head.

3.2 Pneumatic Four-Hole Probes. The cylindrical four-hole probe has a calibration range of ± 30 deg in yaw and ± 24 deg in pitch angles. The probe head shape is similar to the standard FRAP probes and the diameter of the probe is 1.8 mm (Fig. 8).

The steady flow properties, φ, γ, P_{tot}, P_{stat}, and M are measured with the 4HP. Information about measurement uncertainties of 4HP are given in the next chapter of this paper.

4 Probe Measurement Uncertainties

Unlike previously used methods, the guide to the expression of uncertainty in measurement (GUM) [32] describes a standardized method, which first converts all uncertainty information into probability distributions. Based on this, it is consistent to use only the Gaussian error propagation formula to derive the overall uncertainty of the result, which represents a level of confidence of 67%. In the case of correlated parameters, cross-correlation coefficients are used to evaluate their combined uncertainty contribution.

Consequently, the final statement of uncertainty of the measurement result contains the limits and the distribution of the expected values. The GUM method uses a term called "expanded" uncertainty, defined as a multiple of the uncertainty distribution and the coverage factor k. In this case, we define k=2. This value represents a level of confidence of 95% if the result is normally distributed and is, therefore, rather conservative.

The GUM-based measurement uncertainties for FRAP-HT, FRAP, and 4HP are given in Table 2. The concept was discussed by Behr [33] and is applied to the range of dynamic head of the axial turbine measurements presented here. The values for the yaw and pitch angles are given as relative uncertainties to the calibration range of ± 24 deg in yaw and ± 20 deg in pitch. The pressure uncertainties are presented relative to the dynamic head.

Fig. 8 Cylindrical four-hole probe (FRAP shape) presented with a match for scale comparison

Table 2 Typical error bandwidth of flow parameters for the three different probes with the same calibration range

Flow property	FRAP-HT (%)	FRAP (%)	4HP (%)
φ	± 1.1	± 1.0	± 0.9
γ	± 2.0	± 1.7	± 1.6
P_{tot}	± 1.1	± 1.0	± 0.9
P_{stat}	± 1.3	± 1.2	± 1.1

5 Experimental Facility and Hot Streak Generator

The experiments for the current investigation have been conducted in the 1.5 stage unshrouded axial turbine test rig at the Laboratory for Energy Conversion of ETH Zurich. A cross sectional view of the turbine module is presented in Fig. 9. A detailed description of the turbine design is given by Behr et al. [28]. Global parameters of the turbine at the design operating point are shown in Table 3 and the characteristics of each blade row are presented in Table 4.

The test rig is equipped with an internally designed hot streak generator (Jenny et al. [34]). The single passage hot streak generator has an inlet duct diameter of 22 mm with an exit wall thickness of 0.5 mm and is operated in equal Ma number mode (compared with the main flow). In order to reduce main flow disturbance, the conical outer shaped injection tube is installed on a vane-shaped support strut. The injection plan is approximately
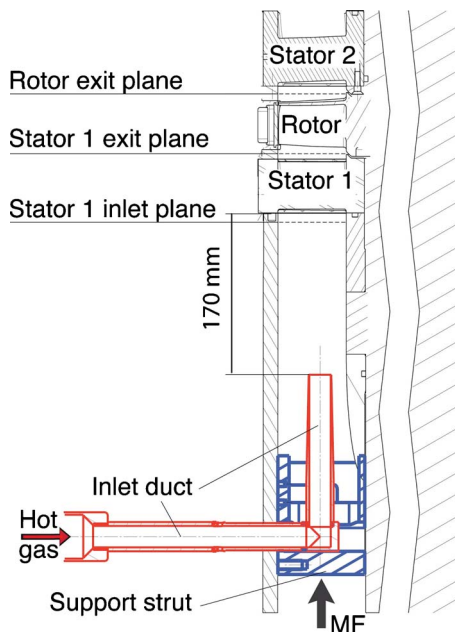

Fig. 9 Close-up view of the one-and-a-half stage unshrouded axial research turbine equipped with a hot streak generator (inlet duct and vane-shaped support strut)

Table 3 Main parameters of LISA 1.5 stage axial turbine research facility at design operating point (measured)

Turbine	
Rotor speed (RPM)	2700
Pressure ratio (1.5 stage, total-to-static)	1.65
Turbine entry temperature (K)	314
Total inlet pressure (bar abs norm)	1.4
Mass flow (kg/s)	11.8
Hub/tip diameter (mm)	660/800

Table 4 Characteristic geometry and performance parameters of the 1.5 stage turbine configuration (performance values are derived from pneumatic probe measurements at the design operating point)

	Stator 1	Rotor	Stator 2
No. of blades	36	54	36
Inlet flow angle (deg) (midspan)	0	54	−42
Exit flow angle (deg) (midspan)	73	−67	64
Aspect ratio (span/chord)	0.87	1.17	0.82
Blade row relative exit Mach numbers (average)	0.54	0.50	0.48
Reynolds number based on true chord and blade row relative exit velocity	7.1×10^5	3.8×10^5	5.1×10^5

3.5 stator axial chords upstream of the first nozzle guide vane. Both the turbine and the hot streak generator are designed such that a variety of parameters can be adapted in order to invest their influence on the flow field. The most interesting parameters are the hot streak temperature, the spanwise position of the hot streak, the shape and size of the hot streak (interface exchange), the pressure of the hot streak, the clocking angle of the stator, and the temperature of the main flow.

The turbine pressure ratio, as well as the main flow entry temperature and the hot streak temperature are kept constant during operation. Daily variations in ambient pressure are considered by nondimensionalizing the measured pressures by the respective total inlet pressure and static outlet pressure. In order to represent real engine conditions, the hot streak mass flow is controlled, such that its stagnation pressure and Mach number are equal to the free stream level.

6 Results and Discussion

In order to prove the concept of the newly developed probe and to allow qualitative and quantitative comparisons to other well-established probes, measurements were performed using a uniform data point grid. One measurement plane consists of 41 traverses for the stator 1 exit plane and the rotor exit plane and due to access issues, 33 traverses for the stator 1 inlet plane. For all measurement planes one traverse contains 45 measurement points. In the case of the stator 1 exit and rotor exit plane, this leads to an overall measurement point density of 1845 points per stator pitch of 10 deg. In the radial direction, the measurement locations range from 5.7% span to the near tip end wall region, located at 99.3% span. Based on the virtual four-sensor probe concept, one measurement point consists of three records, all sampled for 2 s with a data acquisition frequency of 200 kHz. Before and after each radial traverse an offset and gain measurement is performed in the tower position outside the flow by applying two different probe back pressure levels. One measurement plane, therefore, consists of 5699 records, which results in 71.3 GB of raw data per measurement plane and lasts for approximately 10 h.

In the first step of the data processing, the raw data are phase-locked based on one specific trigger position on the rotor circumference. Each resulting data set covers three consecutive passages, containing 82 samples per passage. The previously discussed sensor calibration procedures are applied to the reduced data set. The received pressure signals are then phase-lock-averaged and the aerodynamic calibration model is applied to derive the unsteady flow angles as well as unsteady total and static pressure, Mach number and based on the steady temperature (10 Hz), the velocity components.

Measurements are conducted at the inlet of the first stator, the exit of stator one, as well as on the exit of the rotor (Fig. 9). Three different test configurations will be presented within this paper (Table 5).

Table 5 Invested test cases for different hot streak temperatures and different spanwise injection positions

Conf.	T_{MF} (K)	T_{HS} (K)	T_{HS}/T_{MF}	HSG span position (%)
1	314	378	1.21	50
2	314	429	1.36	50
3	314	429	1.36	20

The hot streak generator was positioned at two different radial locations: at 50% span and at 20% span. Circumferentially, the HSG was positioned at midpitch, in order to avoid a direct impingement onto the blades of the first stator. The measured spanwise distribution of the pitchwise mass-averaged stagnation to main flow temperature ratio $T_{tot,mav}/T_{MF}$ is presented in Fig. 10 for test configurations 2 and 3. The variation in the maxima for the two cases is related to the variation in the HS due to the wall proximity.

6.1 Steady Hot Streak Inlet Conditions. At the inlet of the first stator, the focus of the FRAP-HT measurements is to demonstrate the capability to measure the steady temperature.

Figure 11 represents the steady temperature normalized by the main flow temperature. Measurements performed at the stator inlet with the FRAP-HT probe for configurations 2 and 3 are compared with ideal case simulations at the HS injection plane further upstream. In the simulation of the ideal case, the HS was positioned midpitch of the first stator. However, the measured temperature profiles at the first stator inlet plane show a slight shift of the HS core (−0.05 stator pitch position) compared with the target position of zero pitch. The profiles are circularly shaped for configuration 2 and slightly squeezed in the measurement for configuration 3. The difference in shape is related to wall proximity effects. Another reason for the squeezed shape of the hot spot at 20% span could be related to a slight misalignment of the HS inlet duct compared with the main flow streamlines. The inlet duct is positioned from outside of the turbine casing. The vane-shaped support strut gives guidance for accurate positioning. However, the high thermal gradients could lead to some warping of the duct structure. Any misalignment of the duct compared with the free stream would then lead to a jet in crossflow, resulting in a deflection of the jet in the direction of the crossflow.

For both configurations, the HS core to free stream stagnation temperature ratio is at the same level as at the injection plane
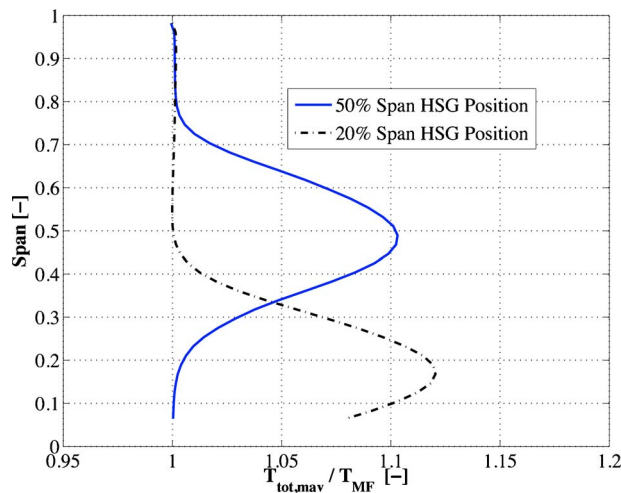

Fig. 10 Normalized total temperature $T_{tot,mav}/T_{MF}$ measured with FRAP-HT at the inlet of stator 1 (pitchwise mass-averaged) for configurations 2 and 3

($T_{tot}/T_{MF}=1.36$). This, as well as the squeezed and, therefore, wider temperature profile of the 20% span HS position, is further illustrated in Fig. 12(a), where a pitchwise cut through the area plots of Fig. 11(b) and 11(d) is represented for T_{tot}/T_{MF} at the respective HS span position.

As shown in the measurements presented in Fig. 11, the temperature at the boundary regions of the HS is reduced. The dissipation of the hot jet is related to mixing effects in the shear layer and to the turbulent temperature profile in the injection pipe flow. An identification of the jet dissipation and the entrainment of the cold flow by the jet is done by a pitchwise cut through the jet cores in Fig. 12(b), showing the typical change in sign of the yaw angle in the core of the respective jet.

6.2 Comparison Between Various Probe Measurement Techniques. Four parameters define the flow: total and static pressures and the yaw and pitch flow angles. In Fig. 13 the pitchwise averaged difference between the results measured with a 4HP, a standard FRAP and the FRAP-HT are brought together for test case configuration 1 at the exit of stator 1. The 4HP measurements are used as a baseline and for both fast response aerodynamic probe measurements the differences are defined with respect to the pneumatic baseline measurements. The presented combined error bandwidth for the respective property is defined out of the sum of the error bandwidth for the 4HP and the FRAP-HT.

All results for the flow angles are within the error bandwidth (Fig. 13(a)). Comparing P_{tot} and P_{stat}, except for a small region at around 10% span, the FRAP-HT results are within the error bandwidth (Fig. 13(b)). Figure 13(a) shows differences of yaw angle for the FRAP ranging from −0.65 deg to 0.5 deg and for the FRAP-HT in the range of −0.55 deg to 0.4 deg. This is considered to be a good agreement. The pitch angle difference for the FRAP ranges from −1.2 deg to −0.25 deg and for the FRAP-HT from −0.8 deg to 0.25 deg. This is consistent with Table 2, which shows that errors in pitch angle are expected to be larger than those for the yaw angle. Focusing on the FRAP-HT measurements, both flow angles show a change in difference close to the tip radius, where the shear layer is located. A combination of end wall proximity effects, blockage effects due to the difference in the probe diameter, and high total pressure gradients located near the end walls might be reasons for this.

The difference in nondimensional total and static pressure measurements is presented in Fig. 13(b). All measurement technologies presented measure the pressures as being in good agreement. The level of deviation is small and ranges around 0.003 in P_{tot} and 0.007 in P_{stat} for most parts of the span. Concerning the average static pressure level, the FRAP-HT shows slightly higher spanwise variations compared with the standard FRAP.

In order to show the capability to resolve unsteady flow structures, the unsteady results are compared between FRAP and FRAP-HT. A Cpt time snapshot at t/T=0.41 over one stator pitch measured with FRAP-HT is presented in Fig. 14(a) for test configuration 1. It shows the interaction between the stator exit flow field and the potential field of the passing rotor (zones of increased Cpt), as well as the secondary flow features that leave the stator blade row (areas of reduced Cpt). The core of the stator hub passage vortex reaches from the hub casing wall up to 10% span. The stator passage vortex can be found at between 80% and 90% span. Both vortices are connected by the stator wake, which exhibits a straight shape and is almost perfectly aligned in the radial direction.

Generally, the flow field out of the stator shows a clear two-dimensional character over a range of 10–70% span. Figure 14(a) further shows that the left-hand stator pitch secondary flows vanish almost completely due to the vicinity of a rotor leading edge, whereas the wake and both vortices are fully developed and approach the midpitch region of two rotor blades in an undisturbed manner on the right-hand stator blade. In this case the total pressure in these areas reaches its minimum value. No direct impact
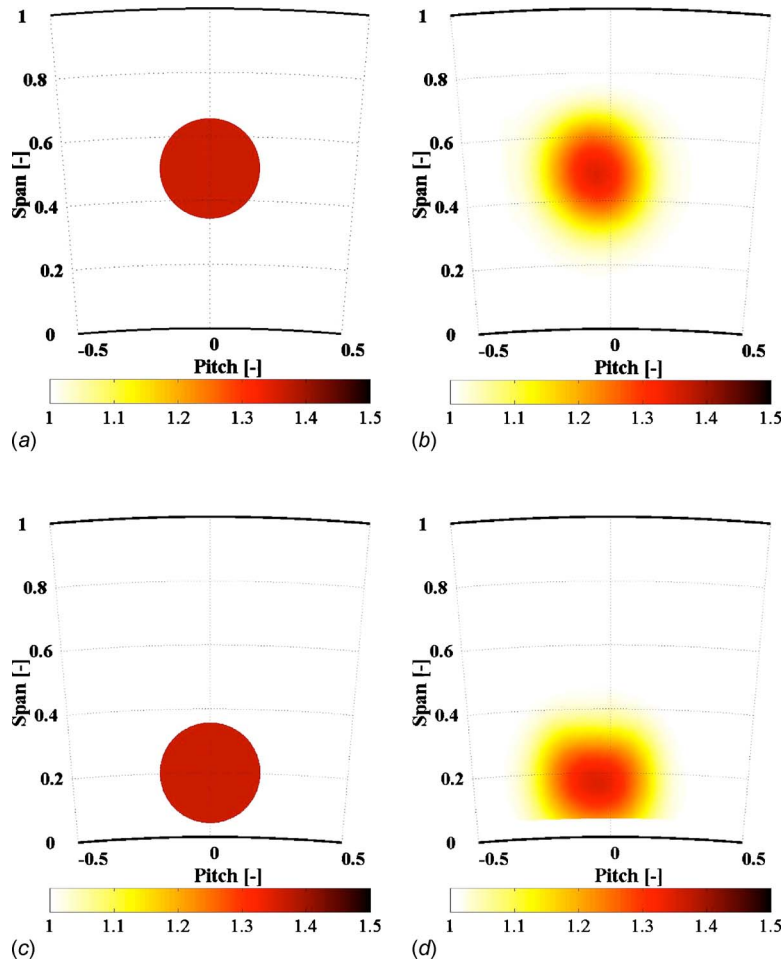
Fig. 11 Steady normalized total temperature (T_{tot}/T_{MF}) over one stator pitch. Ideal case simulation at the HS injection plane for configurations 2 (*a*) and 3 (*c*); FRAP-HT results at the inlet of stator 1 for configurations 2 (*b*) and 3 (*d*).

off the HS can be found in the Cpt distribution around midspan. As already stated by Munk and Prim [35], the measurements obtained show that the secondary flows at the vane exit are not affected by the HS.

Figure 14(*b*) shows the same area but compares rms of the difference in Cpt between FRAP and FRAP-HT for the same sample time t/T. The average of the difference between the two probe technologies scales the result and allows a better comparison between them. Zones of complete agreement between the two measurements, therefore, have an rms of zero. Figure 14(*b*) shows a dominant area of complete agreement. Some small deviations are identified near the tip end wall, in the wake between 60% and 75% span and within the passage vortex regions between 5% and 10% span, and 80% to 95% span, respectively. As previously stated for the mass-averaged differences, a combination of end wall proximity effects, blockage effects due to the difference in the probe diameter and relative sensor position, as well as high total pressure gradients located near the end walls might be reasons for these variations.

Another zone with slight differences is identified between 30% span and 60% span at midpitch. This is the location of the HS and a lower signal to noise ratio of the standard FRAP for elevated flow temperatures could, therefore, be an explanation for the appearance of the deviation zone.

6.3 Unsteady Flow Analysis. The HS-related thermally driven effects on the rotor flow are more complex. In a rotor-

relative frame of reference, the HS has a higher relative momentum and thus a higher relative stagnation pressure. As has been shown by Kerrebrock and Mikolajc [36], this leads to additional sources of secondary flows with the hot gases tending to migrate toward the pressure side and then the end walls. Figure 15 shows the steady T_{tot}/T_{MF} measured with FRAP-HT for the test case configurations 2 and 3 at the rotor exit. The data are presented over one stator pitch and help to identify the time-averaged main location of the HS for later time-resolved area plots at the rotor exit. The span position of the HS core can clearly be identified. Furthermore, the tendency toward an increasingly spanwise distribution of the hot gases on the right-hand side (direction of rotor PS) is identified. A strong shape difference between the steady temperature distributions for the two test cases is shown. The shape for the lower HS span position is much more distorted, which could be related the complex interactions of the hot gas particles with the hub passage vortex and be further influenced by wall proximity effects.

In order to track both the hot streak effects, as well as flow-related unsteady effects such as the wake and vortical structures at the rotor exit, the root mean square value of the random part of the total pressure is presented in Fig. 16 for the HS cases 2 and 3 ($P'_{tot,rms}$). Regions of high $P'_{tot,rms}$ are indicative of eddy shedding or regions of high turbulence. Rotor exit flow measurements are presented over one complete stator pitch. Due to the stator to rotor
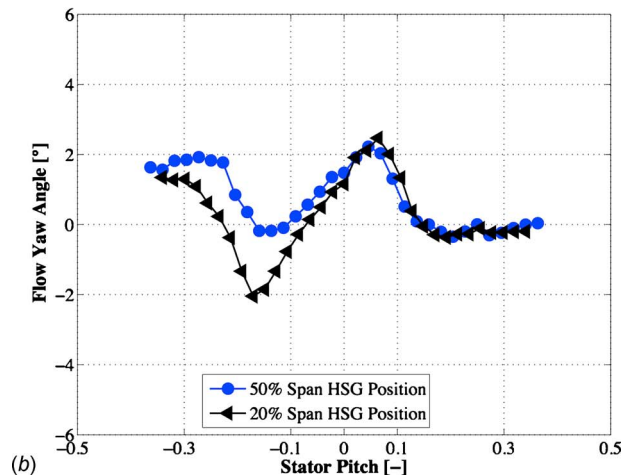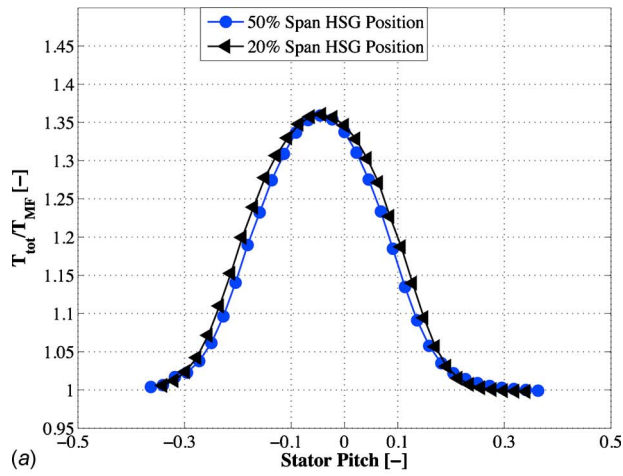
Fig. 12 FRAP-HT pitchwise distribution of time-averaged T_{tot}/T_{MF} (a) and flow yaw angle φ (b) at the span positions of the respective HS core for configurations 2 and 3

Fig. 13 Pitchwise mass-averaged differences of FRAP, FRAP-HT, and 4HP (including error bars). (a) Deviation in flow angles φ and γ and (b) nondimensional pressures. All measured for configuration 1 at the exit of stator 1.

blade count ratio of 2:3, two rotors and their dominating effects are presented within one stator pitch.

Similar $P'_{tot,rms}$ levels occur in the areas of the tip leakage vortex (1), in the area of the upper passage vortex (2) and in the core of the rotor wake (4) for both test cases. The rms level for the hub passage vortex shows an increase in size and intensity for the second test case (3) (Fig. 16(b)). This is mainly related to the hot gas area (5) being located at around 20% span for measurement configuration 3, influencing the secondary flows and, therefore, the hub passage vortex located at the same span position. Furthermore, the migration of the HS toward the PS of the rotor and subsequently toward the end walls is recognizable in zone 5 for both test cases.

7 Concluding Remarks

A novel high temperature fast response aerodynamic probe has been developed, built and tested. The FRAP-HT probe is based on the virtual four-sensor probe measurement concept. The probe can be applied in flows with temperatures up to 533 K (500°F) and can measure three-dimensional and unsteady flows up to the cut-off frequency of 25 kHz, covering flow angles of ±24 deg in yaw and ±20 deg in pitch direction. Furthermore, the probe is able to capture the steady flow temperature.

The probe robustness and capability to provide steady temperature and high frequency flow measurements in harsh environments is demonstrated within the hot streak generator equipped axial 1.5 stage turbine facility, LISA. The combination of that high work
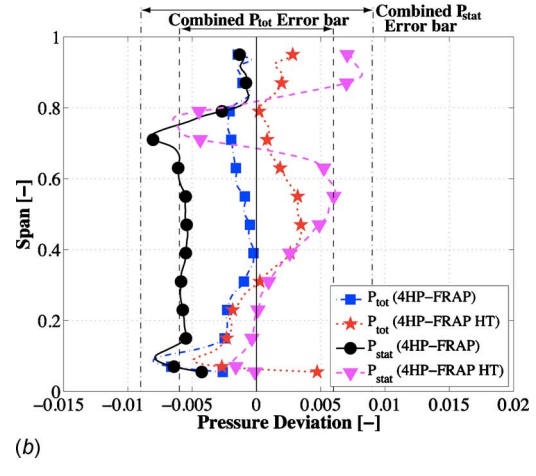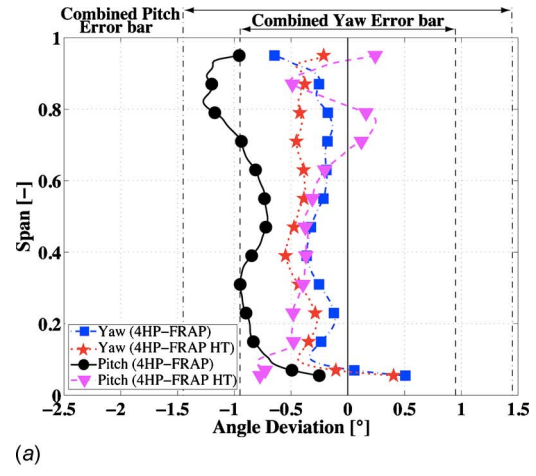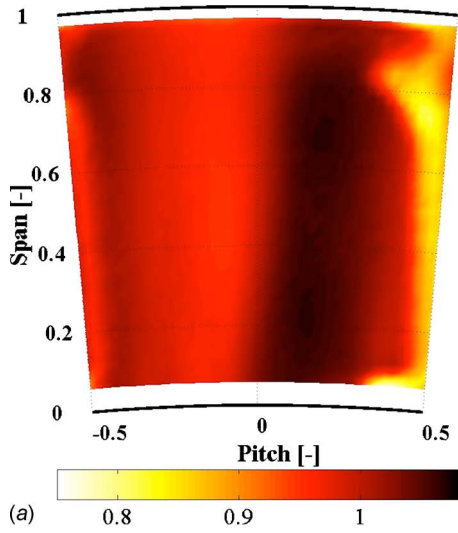
aero-engine and hot gas spots leads to sharp temperature gradients within the flow and to interactions with the blade row pressure gradients and secondary flows and, therefore, presents a perfect scenario to verify the probe's ability to measure under real conditions.
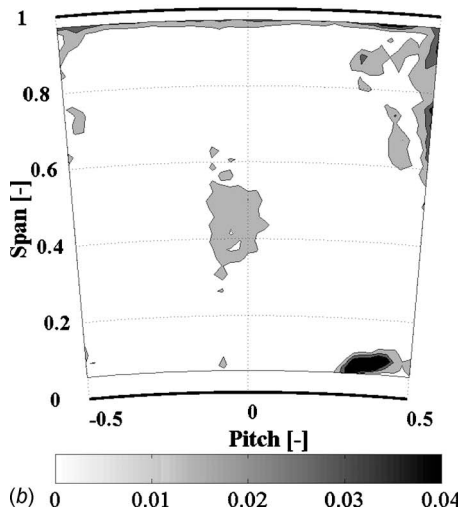
The steady hot streak inlet conditions show equal HS core temperatures compared with the temperatures at the injection plan. The trends of the hot jet dissipation and the entrainment of the cold flow by the jet are shown by the reduced gradients at the HS boundary area upstream of the first stator.

A comparison between measurements using the newly developed high temperature probe against various well-established steady and unsteady measurement techniques is performed. Agreement between all the techniques has been found and, therefore, the new probe concept was proven to be applicable. The minor variations between the results for the different probe techniques might be related to combinations of different effects such as, wall proximity effects, blockage effects due to the difference in the probe diameter and relative sensor position, high total pressure gradients near the end walls and a lower signal to noise ratio of the standard FRAP for elevated flow temperatures compared with the new FRAP-HT.

In terms of the unsteady flow analysis, the Munk and Prim principle [35], stating that the HS does not affect the secondary flows at the vane exit, is verified for the measurements performed. The flow analysis at the rotor exit further shows the interactions between the HS-related thermally driven effects and the unsteady
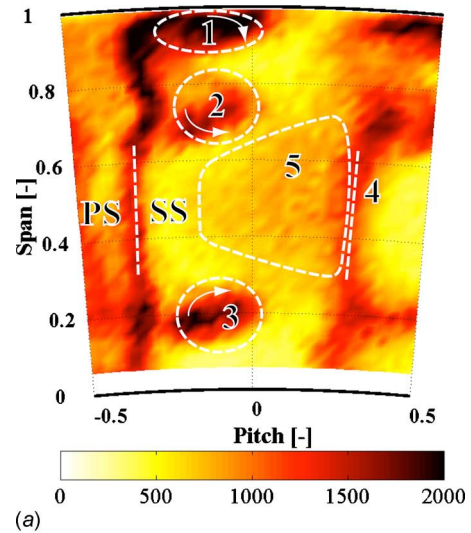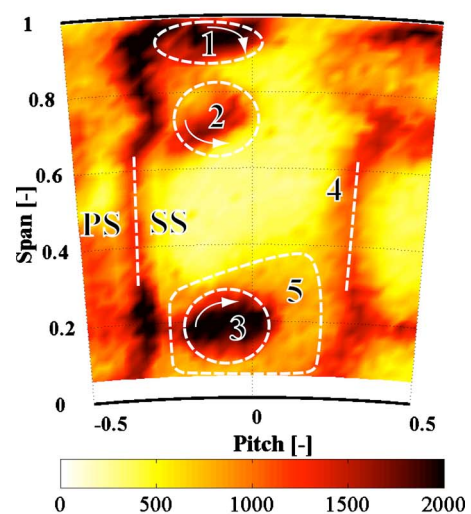
Fig. 14 Time resolved (t/T=0.41) area plot at the exit of stator 1 measured for configuration 1 (absolute frame of reference); (a) Cpt measured with FRAP-HT. (b) Difference in Cpt FRAP and FRAP-HT, expressed by the rms at the same sample time.
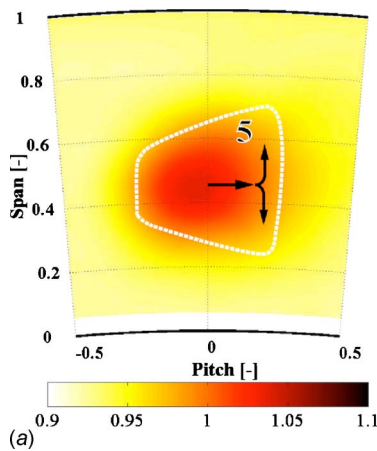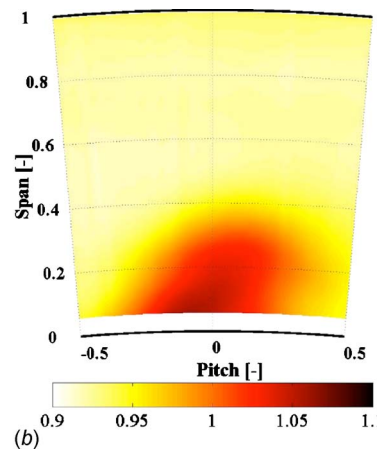

Fig. 16 Time resolved (t/T=0.85) area plot at the exit of the rotor measured with FRAP-HT and presented over one stator pitch (absolute frame of reference). (a) rms of the random part of P_{tot} for configuration 2 and (b) rms of the random part of P_{tot} for configuration 3.

Fig. 15 Steady normalized total temperature (T_{tot}/T_{MF}) over one stator pitch measured with FRAP-HT at the exit of the rotor for configurations 2 (a) and 3 (b).

flow. Kerrebrock and Mikolajc [36] observed the migration of the hot gases toward the rotor pressure side and subsequently toward the end walls. These effects are identified and visualized in the FRAP-HT measurements by time-resolved area plots of the turbulent fluctuating part of the total pressure.

Acknowledgment

Nomenclature

C_{pt} = total pressure coefficient
$C_{pt} = (p_{tot} - p_{stat,3})/(p_{tot,0} - p_{stat,3})$
f = frequency (Hz)
P, p = pressure (Pa)
T_{tot}/T_{MF} = stagnation to main flow temperature ratio
T_{HS} = hot streak core temperature (K)
t/T = time over blade period
U = sensor signal voltage (V)
U_e = sensor excitation voltage (V)

Greek

φ = flow pitch angle (deg)
γ = flow yaw angle (deg)

Abbreviations

conf = configuration
rms = root mean square
HS = hot streak
HSG = hot streak generator
PS = pressure side
SS = suction side
4HP = pneumatic four-hole probe

Subscripts

0 = turbine inlet
3 = turbine exit
HS = hot streak
mav = mass-averaged
MF = main flow
stat = static
tot = total

Superscripts

' = turbulent fluctuation
$-$ = mean value

References

[1] Ainsworth, R. W., Miller, R. J., Moss, R. W., and Thorpe, S. J., 2000, "Unsteady Pressure Measurement," Meas. Sci. Technol., **11**(7), pp. 1055–1076.
[2] Kupferschmied, P., Koppel, P., Gizzi, W., Roduner, C., and Gyarmathy, G., 2000, "Time-Resolved Flow Measurements With Fast-Response Aerodynamic Probes in Turbomachines," Meas. Sci. Technol., **11**(7), pp. 1036–1054.
[3] Sieverding, C. H., Arts, T., Denos, R., and Brouckaert, J. F., 2000, "Measurement Techniques for Unsteady Flows in Turbomachines," Exp. Fluids, **28**(4), pp. 285–321.
[4] Rohlik, H., 1983, *Current and Future Technology in Radial and Axial Gas Turbines*, National Aeronautics and Space Administration, Washington, DC.
[5] Hauser, C., Haas, J., Reid, L., and Stepka, F., 1979, "Turbomachinery Technology," Aeropropulsion (SEE N 80-10205 01-07), pp. 231–272.
[6] Tanaka, H., 1983, "A Survey on Gas Turbine Technology and Research Work in Japan," *Proceedings of the International Gas Turbine Congress*.
[7] Swihart, J., 1987, "U. S. Aeronautical R & D Goals-SST: Bridge to the Next Century," Eighth International Symposium on Air Breathing Engines, pp. 55–65.
[8] Rosen, R., and Facey, J., 1987, "Civil Propulsion Technology for the Next Twenty-Five Years," Eighth International Symposium on Air Breathing Engines, pp. 3–13.
[9] Cook, S. C. P., 1989, "The Development of a High Response Aerodynamic Wedge Probe and Use on a High-Speed Research Compressor," Ninth International Symposium on Air Breathing Engines.
[10] Epstein, A. H., 1985, "High Frequency Response Measurements in Turbomachines," *Measurement Techniques in Turbomachines*, (von Karman Institute Lectures Series), von Karman Institute, Belgium.
[11] Heneka, A., 1983, *Entwicklung und Erprobung einer Keilsonde für instationäre dreidimensionale Strömungsmessungen in Turbomaschinen*, University of Stuttgart, Stuttgart, Germany.
[12] Kerrebrock, J., Epstein, A., and Thompkins, W., Jr., 1980, "A Miniature High Frequency Sphere Probe," *Proceedings of ASME Symposium in Measurement Methods in Rotating Components of Turbomachinery*, pp. 91–97.
[13] Kupferschmied, P., Koppel, P., Roduner, C., and Gyarmathy, G., 2000, "On the Development and Application of the Fast-Response Aerodynamic Probe System in Turbomachines—Part 1: The Measurement System," ASME J. Turbomach., **122**(3), pp. 505–516.
[14] Larguier, R., 1981, "Experimental-Analysis Methods for Unsteady Flows in Turbomachines," ASME J. Eng. Power, **103**(2), pp. 415–423.
[15] Gossweiler, C. R., Kupferschmied, P., and Gyarmathy, G., 1995, "On Fast-Response Probes. Part 1: Technology, Calibration, and Application to Turbomachinery," ASME J. Turbomach., **117**(4), pp. 611–617.
[16] Humm, H. J., Gossweiler, C. R., and Gyarmathy, G., 1995, "On Fast-Response Probes: Part 2: Aerodynamic Probe Design Studies," ASME J. Turbomach., **117**(4), pp. 618–624.
[17] Persico, G., Gaetani, P., and Guardone, A., 2005, "Design and Analysis of New Concept Fast-Response Pressure Probes," Meas. Sci. Technol., **16**(9), pp. 1741–1750.
[18] Ainsworth, R. W., Allen, J. L., and Batt, J. J. M., 1995, "The Development of Fast Response Aerodynamic Probes for Flow Measurements in Turbomachinery," ASME J. Turbomach., **117**(4), pp. 625–634.
[19] Denton, J. D., 1993, "The 1993 IGTI Scholar Lecture—Loss Mechanisms in Turbomachines," ASME J. Turbomach., **115**(4), pp. 621–656.
[20] Binder, A., and Romey, R., 1983, "Secondary Flow Effects and Mixing of the Wake Behind a Turbine Stator," ASME J. Eng. Power, **105**(1), pp. 40–46.
[21] Schlienger, J., Kalfas, A. I., and Abhari, R. S., 2005, "Vortex-Wake-Blade Interaction in a Shrouded Axial Turbine," ASME J. Turbomach., **127**(4), pp. 699–707.
[22] Doorly, D., 1988, "Modeling the Unsteady Flow in a Turbine Rotor Passage," ASME J. Turbomach., **110**(1), pp. 27–37.
[23] Sharma, O. P., Pickett, G. F., and Ni, R. H., 1992, "Assessment of Unsteady Flows in Turbines," ASME J. Turbomach., **114**(1), pp. 79–90.
[24] Philofsky, E., 1970, "Intermetallic Formation in Gold-Aluminum Systems," Solid-State Electron., **13**, pp. 1391–1394.
[25] Kupferschmied, P., 1998, "Zur Methodik zeitaufgeloester Messungen mit Stroemungssonden in Verdichtern und Turbinen," Ph.D. dissertation, ETH Zurich.
[26] Johansen, E. S., and Rediniotis, O. K., 2002, "Development of Unsteady Calibration Facilities and Techniques for Fast-Response Pressure Probes," Fortieth AIAA Aerospace Sciences Meeting and Exhibit, Jan. 14–17.
[27] Harris, C. M., 2002, *Harris' Shock and Vibration Handbook*, McGraw-Hill, New York.
[28] Behr, T., Kalfas, A. I., and Abhari, R. S., 2007, "Unsteady Flow Physics and Performance of a One-and-1/2-Stage Unshrouded High Work Turbine," ASME J. Turbomach., **129**(2), pp. 348–359.
[29] Behr, T., Porreca, L., Mokulys, T., Kalfas, A. I., and Abhari, R. S., 2006, "Multistage Aspects and Unsteady Effects of Stator and Rotor Clocking in an Axial Turbine With Low Aspect Ratio Blading," ASME J. Turbomach., **128**(1), pp. 11–22.
[30] Schuepbach, P., Abhari, R. S., Rose, M. G., Germain, T., Raab, I., and Gier, J., 2008, "Improving Efficiency of a High Work Turbine Using Non-Axisymmetric Endwalls. Part Ii: Time-Resolved Flow Physics," *Proceedings of the ASME Turbo Expo 2008*, Vol. 6, Part A, pp. 1121–1133.
[31] Schuepbach, P., Abhari, R. S., Rose, M. G., Germain, T., Raab, I., and Gier, J., 2008, "Effects of Suction and Injection Purge-Flow on the Secondary Flow Structures of a High-Work Turbine," *Proceedings of the ASME Turbo Expo 2008*, Vol. 6, Part A, pp. 1135–1145.
[32] International Organisation for Standardisation, 1993, *ISO: Guide to the Expression of Uncertainty in Measurement (GUM)*, 1st ed., Geneva, Switzerland.
[33] Behr, T., 2007, "Control of Rotor Tip Leakage and Secondary Flow by Casing Air Injection in Unshrouded Axial Turbines," Ph.D. dissertation, ETH Zurich.
[34] Jenny, P., Lenherr, C., Kalfas, A. I., and Abhari, R. S., 2010, "Effect of Unsteady Blade Row Interaction on Hot Streak Migration in an Axial Turbine," ASME Paper No. GT2010-23034.
[35] Munk, M., and Prim, R., 1947, "On the Multiplicity of Steady Gas Flows Having the Same Streamline Pattern," Proc. Natl. Acad. Sci. U.S.A., **33**(5), pp. 137–141.
[36] Kerrebrock, J., and Mikolajc, A., 1970, "Intra-Stator Transport of Rotor Wakes and Its Effect on Compressor Performance," ASME J. Eng. Power, **92**(4), pp. 359–368.